Available online at www.sciencedirect.com
ScienceDirect
Scripta Materialia 59 (2008) 742–745
Scripta MATERIALIA
www.elsevier.com/locate/scriptamat

Indentation across size scales – A survey of indentation-induced plastic zones in copper {1 1 1} single crystals

M. Rester,* C. Motz and R. Pippan

Erich Schmid Institute of Materials Science, Austrian Academy of Sciences, Jahnstrasse 12, A-8700 Leoben, Austria

Received 6 March 2008; revised 16 April 2008; accepted 3 June 2008
Available online 12 June 2008

The indentation-induced plastic zones below indentations in copper {1 1 1} single crystals, with depths ranging from 250 nm to 250 μm, were examined using electron backscatter diffraction technique. Analyzing the obtained orientation "micrographs" and the corresponding hardness plot exhibits three clearly distinguishable regimes. Comparing the microstructure reflected in the identified regimes to the structure which evolves during the deformation of pure face-centered cubic (fcc) single crystals shows very good agreement.

Keywords: Indentation size effect (ISE); Electron backscatter diffraction (EBSD); Nanoindentation; Microindentation; Macroindentation

For over a century, indentation techniques have been used to measure the hardness of different materials [1]. Depending on the applied forces and consequently the obtained displacements, hardness measurement can be divided into macro-, micro- and nanoindentation.

Macroindentation provides a quick and simple method to obtain the overall bulk hardness of a material and is thus often used in quality control. However, if it is required to identify e.g. the mechanical properties of individual phases or of thin films, macro-hardness measurement is generally not the right method. Micro- and nanoindentation techniques, which apply only small loads, are more appropriate for these tasks. In microindentation, typically pyramid-shaped Knoop or Vickers indenters are used for indentation testing. Dividing the applied load by the surface of the residual impression measured in a microscope, yields the hardness of the material. The typical length scale of the penetration depth is for microindentation in the order of microns. In nanoindentation tests, however, the applied loads and consequently the depth of indentations are further reduced [2–4]. As a result, a direct measurement of the residual impression is no longer possible. This problem can be solved using instrumented indentation testing (IIT), where the area of contact is determined by measuring the depth of penetration of the indenter into the specimen surface [5]. Due to this development, nanoindentation has become a major tool to investigate the mechanical properties of small-scale volumes.

Comparing results of indentation tests at scales from a few hundreds of microns to a few nanometres shows that the hardness increases with decreasing indentation depth. In particular, at the submicron scale the depth dependency of the hardness is highly pronounced. This phenomenon is indicated as indentation size effect (ISE) and is well known from numerous indentation studies [6–10]. In order to explain the observed ISE, great attempts are made to get insight into the indentation-induced deformation behaviour. Particularly the implementation of focussed ion beam (FIB) and electron backscatter diffraction (EBSD) techniques have facilitated a more accurate examination of the deformation zone beneath the imprint. Kiener et al. [11], for example, used conventional EBSD technology to investigate the deformed volume beneath Vickers indentations of depths between 2.4 μm and 700 nm. Zaafarani et al. [12], on the other hand, applied 3D-EBSD technology to examine the texture and microstructure below a 900 nm deep spherical indentation. A similar study, but on a much larger imprint, was performed by Kysar et al. [13], who analyzed the crystal lattice rotations of an approximately 400 μm deep wedge indentation using a conventional EBSD device. Summing up the results of the already performed EBSD studies shows that a wide range of indentation depths is covered. However, one matter which complicates a direct comparison of the

* Corresponding author. Tel.: +43 (0) 3842 804 313; fax: +43 (0) 3842 804 116; e-mail: martin.rester@stud.unileoben.ac.at

1359-6462/$ - see front matter © 2008 Acta Materialia Inc. Published by Elsevier Ltd. All rights reserved.
doi:10.1016/j.scriptamat.2008.06.003

results is the fact that various indenter geometries, as well as different oriented single crystals, were used in these experiments. In order to eliminate these restrictions and to ensure comparability, a survey across size scales of indentation-induced plastic zones below imprints of identical geometry, performed on equally oriented single crystals, would be of great interest.

In the present paper we report a study where the microstructure beneath cube corner imprints from nanoindentations up to macroindentations is investigated. The covered penetration depth thereby reaches from 250 nm to 250 μm, which correspond to loads from 500 μN to 100 N. All indentations were performed on copper single crystals with an $\langle 1\bar{1}0\rangle\{1\,1\,1\}$ orientation. The single crystals were all wet ground and mechanically polished, using alumina suspension with a grain size of 1 μm. Additionally the {1 1 1} surface planes were electropolished to remove any deformation layer caused by mechanical polishing. In order to obtain a sharp edge, the plane perpendicular to the {1 1 1} surface was subsequently carefully mechanically polished. Using three different indentation devices, several cube corner indentations were produced in the vicinity of the polished edge. The smallest indentations, those with loads of 0.5, 1 and 10 mN, were performed by means of a nanoindenter (Hysitron TriboScope), while for the 300 mN imprint an in situ microindenter (ASMEC UNAT) was used. The largest indentations with loads of 10 and 100 N were fabricated using a Kammrath & Weiss compression module. Cross-sections through the centre of all imprints were produced using a FIB workstation (LEO 1540 XB). Detailed information concerning the fabrication process and the used milling parameters can be found in Ref. [14]. Using a field emission SEM (LEO 1525) equipped with an EDAX electron backscatter diffraction system, EBSD investigations on the readily polished cross-sections were performed. Since plastic deformation causes changes of the crystal orientation, EBSD technique facilitates the visualization of traces of plastic deformation. The orientation changes were calculated using EBSD analysis software and visualized by means of colour-coded misorientation maps.

Additionally to the indentations produced for cross-sectioning, several indentations were made from 40 μN to 100 N in order to determine the hardness of the material. Nanoindentations at loads between 40 μN and 10 mN were performed using a Hysitron Triboscope equipped with a cube corner indenter exhibiting a tip radius of about 40 nm. For every selected load three to five separate indentations were accomplished using a load–time sequence described in Ref. [14]. The plotted error bars in Figures 1 and 3 represent the standard deviation of each set of measurements. The area function of the indenter was determined using the procedure outlined by Oliver and Pharr [15]. Indentations between 50 and 300 mN were accomplished by means of an ASMEC UNAT microindenter. The microindenter was fitted with a cube corner indenter and was operated in load-controlled mode. Each load–time sequence consisted of 100 s loading to maximum load, 10 s holding at peak load, and 46 s unloading including a holding period of 20 s at 10% of the peak load. The material hardness was calculated by dividing the applied force by the area of the residual impression determined by means of a LEO 1525 field emission SEM. Errors arising from sizing the imprint area in the SEM are considered by the plotted error bars. Macroindentations were made in load-controlled mode with a Kammrath & Weiss compression module equipped with a cube corner indenter. Using a loading rate of 2.5 Ns^{-1} and a holding period at peak load of 20 s, loads of 10, 50 and 100 N respectively, were applied. Subsequently, the area of the residual imprints was measured and the hardness calculated. The plotted error bars consider errors which arise from determining the imprint area by means of a light microscope.

The results of the hardness measurement are presented in Figure 1a, where a significant ISE can be observed. Starting with a value of 2.75 GPa at an indentation depth of 35 nm the hardness decreases to a value of approximately 0.6 GPa at a depth of about 250 μm. The arrows plotted in the diagram mark the hardness values of the examined indentations.

The corresponding EBSD misorientation maps performed on the fabricated cross-sections through the imprints are displayed in Figure 2. The inset in Figure 2f shows the position of the imprints with respect to the crystallographic orientation of the single crystal. Since the surface normal of the copper crystal is of type [1 1 1] and the crystallographic direction parallel to the investigated surface is of type $[1\bar{1}0]$, the direction normal to the cross-sections is $\langle 11\bar{2}\rangle$. The azimuthally orientation of the cube corner indenter was chosen in that way, to have one side of the impression parallel to the $\langle 11\bar{2}\rangle$ direction. Furthermore it has to be noticed that

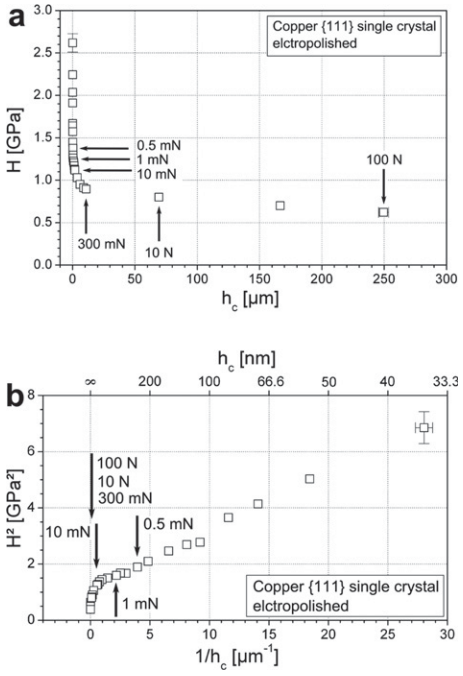

Figure 1. (a) Hardness as a function of indentation depth and (b) square of the hardness as a function of the reciprocal indentation depth, for loads ranging from 40 μN to 100 N. The arrows mark the hardness values of imprints investigated in course of this work. Error bars are inserted only for those datum points where the error bar is larger than the size of the symbol.

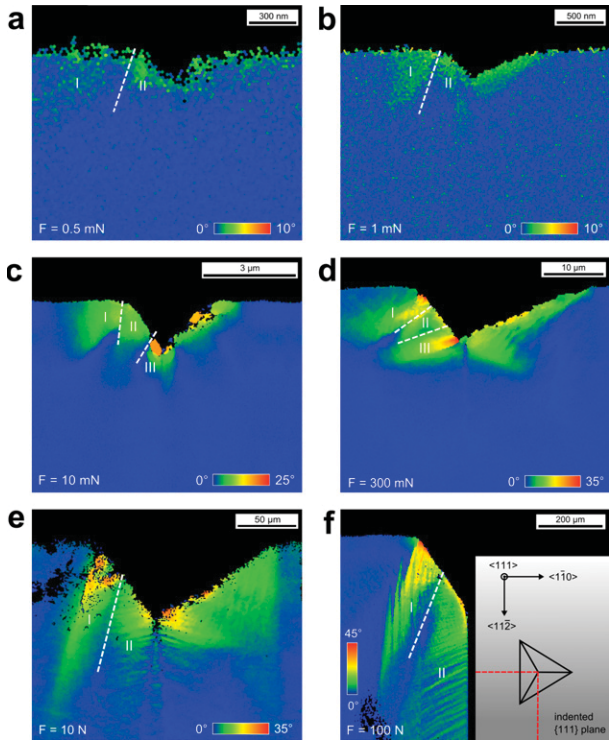

Figure 2. Misorientation maps of indentations in copper for loads of 0.5, 1, 10, 300 mN; 10 and 100 N. The maps (a–e) represent the whole cross-section of the indentations, while for the 100 N indentation only one half of the cross-section is displayed. Noticeable is that in the misorientation maps different colour codes have been used. The inset in (f) shows the position of the imprints with respect to the crystal orientation as well as how the 100 N indentation was cut.

in the following only the left-hand part of the deformation zone is considered, since correct sectioning on the right-hand side, through the imprints edge, cannot be ensured. Starting with the misorientation maps of the smallest sectioned indentations, those made at loads of 0.5 and 1 mN (Fig. 2a and b), shows the formation of patterns consisting of two characteristic sections. As demonstrated in a former work [14], sections I and II are rotated contrary and are separated by a less pronounced arrangement of dislocations. Noticeable is the relatively large lateral extension of section I, as well as the ambiguous character of both sections. This is due to the fact that the misorientation patterns are built up by only few dislocations [16]. Increasing the load and as a consequence the penetration depth yields to a significant increase of the misorientation and to the formation of strongly pronounced patterns (see 10 mN indent in Fig. 2). As can be seen, a third characteristic section denoted III which rotates contrary to section II, appears [14]. Additionally it has to be noticed that in the misorientation maps of the large imprints a less sensitive colour code was used. Compared to the highly ambiguous patterns of the 0.5 and 1 mN imprints, the misorientation patterns of the 10 mN indent look well defined. Analyzing the patterns in the TEM shows for the 10 mN indentation a deformation zone built up by structures of high dislocation density, while the deformation zone of the 0.5 mN indentation consists of only few dislocation loops [16]. It seems that the single dislocations which surround the shallow imprint and induce the observed only slight misorientation gradients are responsible for the ambiguous character of the deformation patterns.

The misorientation map of the 300 mN indentation (Fig. 2d) shows similarity to the 10 mN imprint. Here as well three sections, which characterize the traces of deformation, appear. Differences to the 10 mN imprint can be found in a much more confined section II and in a vertical line below the imprints tip associated with the already know change of the shear stress field. Figure 2e represents the misorientation map of a 10 N imprint. Investigating the map, shows that only two characteristic sections appear. Interesting is the high axial and an only minor lateral extension of section I. Section II, on the other hand, is axially more limited. As can be seen, the deformation pattern in section II is axially extended by slip bands which are symmetrically arranged at the centreline. Laterally section II is enclosed by the changing shear stress field on the right-hand side and by the deformation pattern of section I on the left-hand side. The deformation-induced zone of the largest investigated indentation, performed at a load of 100 N, is displayed in Figure 2f. Of note is that only the left-hand side of the imprint was cross-sectioned, in order to keep the FIB milling time down. As already found for the 10 N indentation, here as well the deformation-induced zone consists of two characteristic sections. Both sections are laterally strongly confined, while axially they reach far into the bulk. Noticeable is the strong fragmentation of the deformation pattern into substructures.

It has to be mentioned that the described changes in the evolution of the microstructure are not reflected in the hardness curves presented in Figure 1, neither in the H vs. h_c plot (a) nor in the H^2 vs. $1/h_c$ plot (b). However, replotting the data in a logarithmic diagram shows three clearly distinguishable regimes (see Fig. 3). Comparing the identified regimes denoted by α, β and γ, to the different "structure–formation" processes found in Figure 2, show very good agreement. In regime α, where the imprints are smaller than approximately 300 nm, no significant orientation changes were detected (Fig. 2a). Regime β, which describes indentations between 300 nm and 30 µm in depth, is characterized by

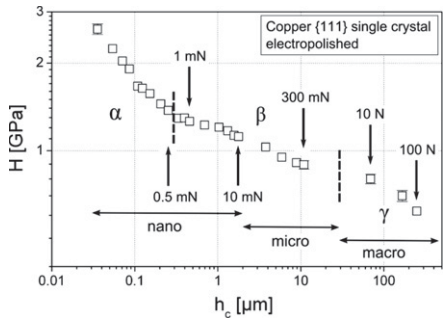

Figure 3. Logarithmic plot of the hardness versus the indentation depth for loads ranging from 40 µN to 100 N. The arrows mark the hardness values of imprints investigated in course of this work. Error bars are inserted only for those datum points where the error bar is larger than the size of the symbol.

regions exhibiting distinctive changes of the orientation (Fig. 2c and d). Noticeable is that in this regime the dimension of the misorientation patterns are proportional to the size of the imprint. Furthermore, the orientation differences increases with growing indentation depth, especially between 300 nm and 1 μm. Regime γ, on the other hand, associated with indentations larger than 30 μm, is indicated by a substructure which typically forms during the deformation of fcc single crystals of pure metals (Fig. 2e and f). In order to facilitate the subsequent discussion, in the following the salient fundamental features of strain hardening behaviour of single crystals are listed:

- The hardening behaviour of a single crystal shows different stages, denoted I, II, III, IV and V.
- The onset-stress for plastic deformation of fcc single crystals of pure metals is very low and their flow stress exhibits an extraordinary high hardening capacity.
- The dislocation structure developed in a single crystal depends significantly on the applied strain and the path the straining is accomplished. It usually starts by the formation of micro- and macro-slip bands and proceeds by the generation of cells and cell block structures. Further deforming keeps the process of fragmentation on. Finally, at very large strains a saturation structure with a minimum crystallite size is reached. For copper single crystals deformed at room temperature, this crystallite size is in the order of a few 100 nm [17].
- Additionally it has to be considered that in case the imprint size is significantly larger than the dimension of the deformation-controlling microstructure, the hardness should be independent of the imprint size.

Keeping the aforementioned facts in mind, it becomes evident that the size of the investigated imprints covers a wide range of the different scales of structural evolution which occur during the deformation of a single crystal. Due to these facts it is not surprising that hardness changes with the size of indentation. As can be seen, regime α is characterized by an imprint size which is lower than the smallest structural element of a single crystal deformed at very large strains. At such small imprints no substructure, which exhibits large misorientation gradients, is generated. It is assumed that the indentation is realized by dislocation loops, pushed into the crystal, building up a "prismatic loop-like" structure. Since the loops arrange in a very widespread manner, the resulting orientation changes are only small [14,16,18]. In this regime, plastic flow is controlled by the source stress and the back stress of already existing dislocations. Regime β is characterized by substructures, which are typical for heavy plastically deformed single crystals. The dimensions of these structures are dependent on imprint size and the amount of misorientation between the different regions. As demonstrated in Figure 2, augmentation of the indent size yields to an increased size of the substructure. It seems that the increasing substructure size is responsible for the decreasing hardness, similar to the observed decrease of flow stress with increasing grain size. The characteristic of regime γ are regions with a substructure similar to low and medium deformed single crystals. It can be seen from Figure 2e and f that these regions, exhibiting a structure that typical develops in a single crystal at low strains, become more and more important. This already known fact [19] seems to be responsible for a further reduction of the hardness. In the authors' opinion the very low stress necessary for the onset of plasticity in pure fcc metals, the very high hardening capacity and the formation of different substructures causes the ISE for the relatively large imprints.

Summarizing, the following conclusions can be drawn. The hardness of a material varies with the size of the indent, as the flow stress of a single crystal with the evolving substructure. Only for very small imprints (i.e. in regime α), the source size becomes the dominant effect.

This work was financially supported by the FWF (Fonds zur Förderung der wissenschaftlichen Forschung) through Project P 17375-N07.

[1] D. Tabor, The Hardness of Metals, Clarendon Press, Oxford, 1951.
[2] J.B. Pethica, R. Hutchings, W.C. Oliver, Philos. Mag. A 48 (1983) 593.
[3] M.F. Doerner, W.D. Nix, J. Mater. Res. 1 (1984) 601.
[4] W.C. Oliver, R. Hutchings, J.B. Pethica, Measurements of hardness at indentation depths as low as 20 nanometers, in: P.J. Blau, B.R. Lawn (Eds.), Microindentation Techniques in Materials Science and Engineering, Spec. Tech. Publ. 889, American Society for Testing and Materials, Philadelphia, 1986, p. 90.
[5] A.C. Fischer-Cripps, Nanoindentation, Springer, New York, 2004.
[6] W.D. Nix, H. Gao, J. Mech. Phys. Solids 46 (1998) 411.
[7] N. Gane, J.M. Cox, Philos. Mag. A 22 (1970) 881.
[8] Q. Ma, D.R. Clarke, J. Mater. Res. 10 (1995) 853.
[9] N.A. Stelmashenko, M.G. Walls, L.M. Brown, Y.V. Milman, Acta Metall. Mater. 41 (1993) 2855.
[10] Y.Y. Lim, M.M. Chaudhri, Philos. Mag. A 79 (1999) 2979.
[11] D. Kiener, R. Pippan, C. Motz, H. Kreuzer, Acta Mater. 54 (2006) 2801.
[12] N. Zaafarani, D. Raabe, R.N. Singh, F. Roters, S. Zaefferer, Acta Mater. 54 (2006) 1863.
[13] J.W. Kysar, Y.X. Gan, T.L. Morse, X. Chen, M.E. Jones, J. Mech. Phys. Solids 55 (2007) 1554.
[14] M. Rester, C. Motz, R. Pippan, Acta Mater. 55 (2007) 6427.
[15] W.C. Oliver, G.M. Pharr, J. Mater. Res. 7 (1992) 1564.
[16] M. Rester, C. Motz, R. Pippan, Mater. Res. Soc. Symp. Proc. 1049 (2007) AA03-03.
[17] M. Hafok, A. Vorhauer, J. Keckes, R. Pippan, Mater. Sci. Forum 503–504 (2006) 621.
[18] D.S. Balint, V.S. Deshpande, A. Needleman, E. Van der Giessen, J. Mech. Phys. Solids 54 (2006) 2281.
[19] F. Schulz, H. Hanemann, Z. Metallk. 33 (1941) 124.